ChemPubSoc Europe

DOI: 10.1002/chem.201700231

CHEMISTRY A European Journal Full Paper

Computational Chemistry

Computational Study of Oxidation of Guanine by Singlet Oxygen ($^1\Delta_g$) and Formation of Guanine:Lysine Cross-Links

Bishnu Thapa,[a] Barbara H. Munk,[a] Cynthia J. Burrows,[b] and H. Bernhard Schlegel*[a]

Abstract: Oxidation of guanine in the presence of lysine can lead to guanine–lysine cross-links. The ratio of the C4, C5 and C8 crosslinks depends on the manner of oxidation. Type II photosensitizers such as Rose Bengal and methylene blue can generate singlet oxygen, which leads to a different ratio of products than oxidation by type I photosensitizers or by one electron oxidants. Modeling reactions of singlet oxygen can be quite challenging. Reactions have been explored using CASSCF, NEVPT2, DFT, CCSD(T), and BD(T) calculations with SMD implicit solvation. The spin contamination in open-shell calculations were corrected by Yamaguchi's approximate spin projection method. The addition of singlet oxygen to guanine to form guanine endoperoxide proceeds step-wise via a zwitterionic peroxyl intermediate. The subsequent barrier for ring closure is smaller than the initial barrier for singlet oxygen addition. Ring opening of the endoperoxide by protonation at C4–O is followed by loss of a proton from C8 and dehydration to produce 8-oxoG^{ox}. The addition of lysine (modelled by methylamine) or water across the C5=N7 double bond of 8-oxoG^{ox} is followed by acyl migration to form the final spiro products. The barrier for methylamine addition is significantly lower than for water addition and should be the dominant reaction channel. These results are in good agreement with the experimental results for the formation of guanine–lysine cross-links by oxidation by type II photosensitizers.

Introduction

DNA can be damaged by a wide variety of reactive oxidation species, such as hydroxyl radical, peroxyl radical and singlet oxygen. Singlet molecular oxygen ($^1O_2$) can be generated from diverse processes such as the type II photosensitization, thermal decomposition of peroxides and other chemical reactions.[1–3] Photosensitization involves a transfer of energy sufficient to excite triplet ground state molecular oxygen, $^3O_2$ ($^3\Sigma^-_g$) to its lowest excited singlet state ($^1\Delta_g$).[4,5] Due to its highly electrophilic nature, singlet molecular oxygen is capable of oxidizing a wide range of molecules including phenols, sulfides, and amines. When it is present in a cellular environment, singlet oxygen can react with nucleobases and amino acids. The most frequent target of oxidative attack on nucleobases is guanine since it has the lowest oxidation potential. The reaction of singlet oxygen with guanine in DNA leads to the formation of various intermediates including 8-oxo-7,8-dihydroguanine (**8-oxoG**). When 8-oxoG is incorporated in DNA, it can alter replication. When other reactive nucleophiles, such as amino acids, are present in the cellular environment, oxidized guanine intermediates can undergo further modifications. A common example is the formation of DNA–protein cross-links (DPC). DPC formation can lead to cellular damage, mutations, cancer, etc.[6–13] Therefore, the reaction of singlet oxygen with DNA and further reactions of oxidatively damaged DNA have been a subject of extensive research.[14–20] In particular, the reactions of singlet oxygen with guanine has drawn significant attention because of the wide variety of reaction pathways, intermediates and products, and their dependence on the reaction conditions and structural context.[14,15,19,21–30]

A large number of experimental studies have investigated oxidative damage of isolated nucleobases, single-stranded and double-stranded DNA by singlet oxygen.[22–34] It is widely accepted that the singlet oxygen addition to the guanine in aqueous solution results in the formation of a guanine endoperoxide intermediate (Scheme 1). In this geometrically strained cyclic intermediate, the 5-membered endoperoxide ring opens to form 8-hydroperoxyguanine (**8-OOH-G**) (atom numbering for guanine is shown in Scheme 2). Dehydration of **8-OOH-G** followed by loss of the C8 proton and rearrangement results in the formation of spiroiminodihydantoin (**Sp**). Alternatively, reduction of 8-OOH-G produces the widely known guanine oxidation intermediate **8-oxoG**, which then can react with O_2 or undergo further oxidation to produce oxidized products such as **Sp**, guanidinohydantoin (**Gh**), and 2,5-diamino-4*H*-imidazolone (**Iz**).[14,16–18] Different reaction conditions such as change in pH, presence of other nucleophiles and additional oxidizing agents along with the singlet oxygen can increase the diversity of the final products.[17,26,30,34] Even

[a] *B. Thapa, Dr. B. H. Munk, Dr. H. B. Schlegel*
Chemistry Department, Wayne State University
Detroit, Michigan 48202 (USA)
E-mail: hbs@chem.wayne.edu

[b] *Dr. C. J. Burrows*
Chemistry Department, University of Utah
Salt Lake City, Utah 84112 (USA)

Supporting information and the ORCID identification number(s) for the author(s) of this article can be found under: http://dx.doi.org/10.1002/chem.201700231.

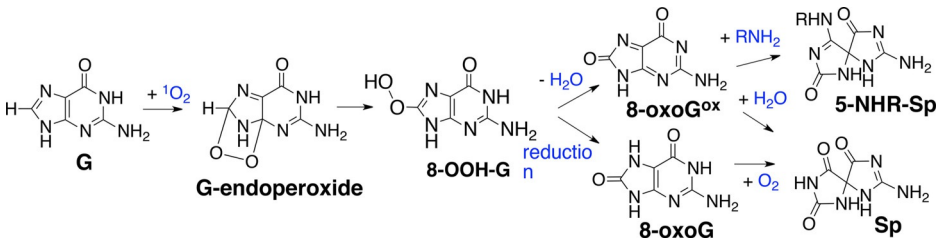

Scheme 1. Formation of spiroiminodihydantoin products from guanine and singlet oxygen in aqueous medium in the presence of lysine.

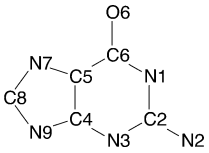

Scheme 2. Numbering of atoms in guanine.

solvent water can act as a nucleophile to react with oxidized guanine intermediates to produce **Sp** and other further oxidized products.[17,23,30,32] It has also been proposed that a second singlet oxygen can react with **8-oxoG** to form **Sp**.[14,17,24–26,35]

The presence of any nucleophiles along with water and/or singlet oxygen can produce a mixture of products including **Sp**.[30,34] A wide range of amino acids including lysine, histamine, and arginine have been found to act as nucleophiles, reacting with oxidized forms of guanine to produce cross-links with DNA bases. The presence of lysine in the reaction mixture has been found to produce predominantly C5-lysine-substituted-**Sp** and to suppress the formation of **Sp**. Similarly, the presence of ammonia favors the formation of C5-NH_2-substituted-**Sp**.[34] The formation of DPC is not limited to oxidation by singlet oxygen. Numerous experimental studies have been carried out to explore the formation of DNA–protein cross-links with isolated nucleobases and single- and double-stranded DNA under different oxidative environments.[12,17,30,36–48] Various oxidizing agents such as hydroxyl radicals, sulfate radicals, carbonate radicals, organic carcinogens such as aldehydes, transition-metal ions such as Ni^{II}, Cr^{VI}, Fe^{II}, Fe^{III}, Ir^{IV}, and ionizing radiation, UV-, and visible light with photosensitizers are also found to induce DPC formation.[30,36–38,40,49–53] The spectrum of the DPC products depends on the nature of the oxidizing agent.[30] In a previous study, we investigated the formation of guanine:lysine cross-links in the presence of benzophenone, a type I photosensitizer.[54] In the present work, we examine the oxidation of guanine by singlet oxygen produced by a type II photosensitizer, and the subsequent formation of guanine:lysine cross-links.

Several theoretical studies have explored the mechanism of singlet oxygen addition reaction across double bonds by using density functional theory (DFT) and multireference methods.[55–66] These studies involve 1,2- or 1,4-type additions of singlet oxygen across double bonds to form an endoperoxide, reactions analogous to the current study. Closed shell single-reference calculations cannot describe singlet oxygen properly because of its multireference character. Broken symmetry, open shell DFT calculations struggle to provide a suitable description of singlet oxygen because of spin contamination from its lower lying triplet state. This can cause sizeable errors in the energy unless spin projection is used to remove the contamination. The problem can exist not just in the reactant but also in the transition states (TSs) and intermediates.[58] Even multi-configuration self-consistent field calculations, that include primarily non-dynamic correlation, can have difficulties because of the lack of dynamic electron correlation, requiring complete active space self-consistent field (CASSCF) calculations along with second order perturbation theory corrections (e.g. CASPT2, NEVPT2, etc.) or multi-reference configuration interaction (MRCI) calculations.[57–59] For example, a study by Sevin and McKee[58] exploring the reaction of singlet oxygen with 1,3-cyclohexadiene showed significant spin contamination in open-shell B3LYP calculations of some of the TSs and intermediates as well as for singlet oxygen, and required CASPT2 calculations to obtain good agreement with the experimental barrier.

Only a few computational studies have explored the reaction mechanism for singlet oxygen addition to guanine. Dumont et al. have examined the performance of various density functionals in calculating the stability of the endoperoxide intermediate versus the zwitterionic peroxyl intermediate, and find that LC-BLYP gives the best agreement with higher level calculations.[67] They have also compared $^1O_2$ addition to guanine and adenine, and find guanine is more readily oxidized than adenine, in agreement with experiment.[68] Dumont et al. used QM/MM calculations and MD simulations to examine guanine oxidation in B-helical DNA and find that the $^1O_2$ addition transition state, the zwitterionic intermediate and the endoperoxide are strongly stabilized by the DNA environment.[68,69] Their DFT study using the LC-BLYP functional with the 6–31+G* and DZP++ basis sets in aqueous solution showed that the 4,8-OO-guanine endoperoxide is formed via a zwitterionic intermediate. However, these DFT calculations did not address spin-contamination from low-lying triplet states in open shell calculations of singlet oxygen and the transition states for addition. This can lead to significant changes in barrier heights and reaction energies. Mendez-Hurtado et al.[70] circumvented the problem of spin contamination in the singlet state of oxygen by using the spin pure triplet state energy and adding the experimental energy that corresponds to the singlet–triplet gap for their study of histidine oxidation by singlet oxygen. This approach eliminates the necessity of dealing with the multireference character of singlet oxygen to some extent. However, the problem still remains since the transition states and intermediates can have significant spin-contamination, and no experimental singlet–triplet gaps are available to correct their energies. In a related study, Lu et al.[71,72] used guided ion-beam mass spectrometry and DFT

calculations to examine the gas phase reactivity of singlet oxygen with protonated and deprotonated guanine. Singlet oxygen addition to protonated guanine produced 5,8-OO-guanine endoperoxide in a concerted reaction, while deprotonated guanine reacted with singlet oxygen in a step-wise fashion and formed 4,8-OO-guanine endoperoxide.

The yield of the various cross-link products between guanine and lysine has been shown to depend on the nature of the oxidizing agent.[30] In our previous study,[54] we investigated the mechanisms for the formation of guanine:lysine adducts in the presence of benzophenone, a type I photosensitizer. The present study explores the oxidation of guanine by singlet oxygen, generated by a type II photosensitizer, and the subsequent reaction pathways for nucleophilic addition of lysine to form guanine:lysine adducts. As discussed above, the DFT calculations of singlet oxygen are problematic due to the spin contamination from its low-lying triplet state. This problem may persist in the TSs and the intermediates following the singlet oxygen addition. Approximate spin projection methods can eliminate the spin contamination from other spin states. In this study, the energies of spin contaminated, broken symmetry (BS) structures are corrected using Yamaguchi's approximate-spin projection method.[63,65] A range of methods (CASSCF, NEVPT2, B3LYP, ωB97XD, LC-BLYP, CCSD(T), and BD(T)) has been used to explore the potential energy surface for singlet oxygen addition to guanine and subsequent reaction with water and lysine. As in our previous studies, the sidechain of lysine is modeled by methylamine (this lowers computational cost without reducing the accuracy). A minimum energy pathway has been identified based on the energies and barriers of each reaction step.

Results and Discussion

Scheme 1 shows the pathways for the addition of singlet oxygen ($^1\Delta_g$) to guanine and the subsequent addition of methylamine or water to form substituted-spiroiminodihydantoin products. The reactions were explored with a range of theoretical methods: DFT, CCSD(T), BD(T), CASSCF and NEVPT2. The treatment of singlet oxygen and its reactions can be challenging for some levels of theory. Since the addition of singlet oxygen to 1,3-cyclohexadiene has been investigated experimentally and computationally, we examine this reaction first in order to calibrate the methods used for singlet oxygen plus guanine. After examining the addition of singlet oxygen to the guanine to form endoperoxide, we looked at the reaction path from the endoperoxide to 8oxoG and nucleophilic addition followed by ring rearrangement to form substituted-spiroiminodihydantoin products.

(a) Addition of singlet oxygen to 1,3-cyclohexadiene

The experimental difference between the singlet and triplet states of oxygen is 22.4 kcal mol^{-1}.[73] Table 1 shows the calculated result for various levels of theory. CASSCF/6–31+G(d,p) calculations with an active space of 12 electrons and 8 orbitals give a singlet–triplet energy gap of 21.5 kcal mol^{-1} for the molecular oxygen (the active orbitals are shown in the Supporting Information). Corrections for dynamic correlation by second order perturbation theory (CASPT2 and NEVPT2) improves the value by a few kcal mol^{-1}. Closed-shell calculation of singlet oxygen at the B3LYP/6–31+G(d,p) level of theory has a spin restricted to unrestricted instability and optimizes to a stable open-shell electronic structure that has a spin-squared value $<S^2>\approx 1.0$. This broken symmetry singlet oxygen has about 50% contribution from the lowest triplet ($^3\Sigma^-_g$) state and is 10.4 kcal mol^{-1} higher than the ground state triplet. Similar spin-contaminations and singlet–triplet energy gaps are calculated with other DFT functionals. Using the Yamaguchi approximate spin-projection method (AP)[74–76] to correct the energy of spin-contaminated open-shell singlet oxygen, the energy difference between singlet and triplet states of oxygen becomes 20–23 kcal mol^{-1} with various DFT functionals,[65] in good agreement with the experimental value. Similarly, CCSD(T), and BD(T) calculations with Yamaguchi approximate spin-projection yield singlet–triplet energy differences within a few kcal mol^{-1} of the experimental value. All the energies discussed below for broken symmetry, open-shell states calculated with DFT, CCSD(T), and BD(T) are corrected to the spin-pure state using the Yamaguchi approximate spin-projection method.

The gas phase energetics for the [4+2] addition of singlet oxygen to 1,3 cyclohexadiene to form the endoperoxide have been computed with B3LYP, ωB97XD, LC-BLYP, BD(T), CASSCF and NEVPT2, and are compared with experimental[77] and calculated[58] results from the literature in Table 1. The relative energies calculated using CASSCF/6–31+G(d,p) with an active space of 16 electrons in 12 orbitals are lowered by 10–20 kcal

Table 1. Relative energies (with ZPE) calculated for the formation of endoperoxide from 1,3-cyclohexadiene and singlet oxygen using various levels of theory in the gas phase with the 6–31+G(d,p) basis set.

	B3LYP[a]	ωB97XD[a]	LC-BLYP[a]	BD(T)[a,b]	CASSCF[a,b]	NEVPT2[a,b]	CASPT2[c,d]	Experiment
$^1O_2$–$^3O_2$	20.8	23.50	21.85	19.4	21.5	23.4	24.7	22.4[e]
Reactant	0.00	0.00	0.00	0.00	0.00	0.00	0.00	
TS	3.34	3.21	8.24	10.02	23.58	11.22	6.50	5.50[f]
Intermediate	−9.46	−12.63	−16.79	−3.91	10.58	−5.93	−5.50	
Product	−31.48	−39.59	−47.71	−36.27	−16.86	−39.40	−33.60	

Reactant = 1,3-cyclohexadiene + $^1O_2$, Product = 2,3-dioxabicyclo[2.2.2]oct-5-ene. [a] 6-31+G(d,p) basis set. [b] using B3LYP/6–31+G(d,p) optimized geometry and zero-point energy. [c] 6-31G(d) [d] Ref.[58] [e] Ref[73] [f] Ref.[77]

mol^{-1} when dynamic electron correlation is taken into account by NEVPT2/6–31+G(d,p) and CASPT2/6-31G(d) calculation. The NEVPT2, spin projected BD(T) and spin projected LC-BLYP barriers are 3–6 kcal mol^{-1} higher than experiment while the spin projected B3LYP and ωB97XD barriers are 2 kcal mol^{-1} lower than experiment. Except for CASSCF, the calculations find the intermediate more stable than the reactants and the overall reaction strongly exothermic. Even though the singlet oxygen and the intermediates involved here have multireference character, spin-projected DFT (B3LYP and ωB97XD, in particular) perform reasonably well in predicting the relative energetics for the [4+2] addition of singlet oxygen to 1,3-cyclohexadiene. By extension, B3LYP and ωB97XD functionals plus spin projection should also provide good estimates of the energetics for singlet oxygen addition to guanine to form guanine endoperoxide.

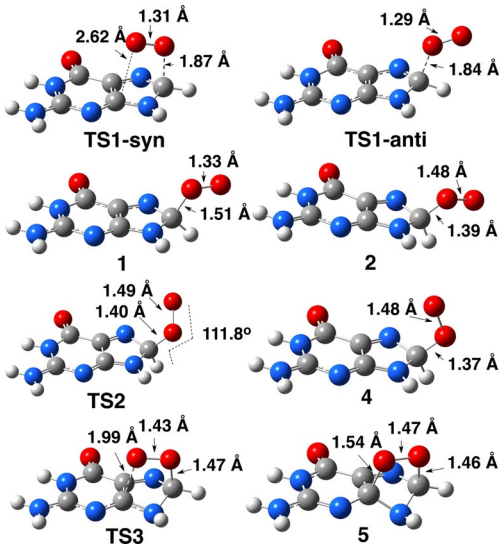

Figure 1. Transition states and intermediates for the formation of guanine endoperoxide optimized with SMD-B3LYP/6–31+G(d,p) in aqueous solution.

(b) Addition of singlet oxygen to guanine and formation of the endoperoxide

Possible pathways of the formation of guanine endoperoxide from singlet oxygen and guanine are presented in Scheme 3 and some of the intermediate structures with relevant bond lengths are shown in Figure 1. The relative enthalpies (Δ*H* at 298 K) are listed in Table 2 and are shown in Figure 2 and Figure 3.

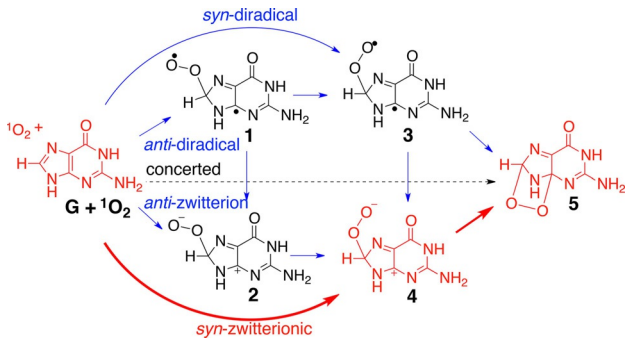

Scheme 3. Addition of singlet oxygen to guanine to form guanine endoperoxide (the most stable structures and lowest energy reaction path are shown in red).

There are two orientations for singlet oxygen addition to the guanine to form the endoperoxide, namely, *syn* and *anti* with respect to the guanine ring. The *anti*-addition is a three-step process while the *syn*-addition can be one step or two steps, as shown in Scheme 3. The *syn*-addition of singlet oxygen could follow a concerted, synchronous Diels–Alder reaction mechanism as has been found in a number of symmetric alternate hydrocarbons such as benzene, naphthalene, and anthracene derivatives.[57,61] However, the concerted [4+2] addition of a singlet oxygen across C8–C4 of guanine is not likely to be synchronous because of the different reactivity of the C8 and C4 sites. A two-dimensional scan of the C4···O and C8···O coordinates is shown in Figure 4. As guanine and singlet oxygen approach each other, they start with similar C4···O and C8···O distances. Shortening the C8···O distance is clearly preferred over shortening the C4···O distance. The latter is unfavorable because it would disrupt the aromaticity of the six-membered

Table 2. Relative enthalpies calculated for the formation of guanine endoperoxide from guanine and singlet oxygen using various levels of theory with the 6–31+G(d,p) basis set in aqueous solution with SMD solvation.

	B3LYP	ωB97XD	LC-BLYP	CCSD(T)[a,b]	BD(T)[a,b]	CASSCF[b] (20e,14o)	CASSCF[a,b] (20e,14o)	CASSCF[a,b] (14e,11o)	NEVPT2a[b] (14e,11o)
G+$^1O_2$	0.0	0.0	0.0	0.0	0.0	0.0	0.0	0.0	0.0
TS1-*syn*	2.8	4.1	8.7	5.8	4.4	16.5	19.5	23.7	7.1
TS1-*anti*	6.5	9.9	13.0	11.4	14.0	32.2	36.9	40.4	19.9
1 (diradical)	2.7	1.3	−0.9	5.0	8.3	29.3	–	35.7	12.9
2(zwitterion)	−3.2	−5.0	−9.3	−4.9	−4.8	10.5	11.7	19.3	9.6
TS2 (diradical)	–	–	–	–	–	29.4	–	–	–
TS2 (zwitterion)	4.4	2.3	-0.9	2.6	2.7	17.8	20.9	25.3	15.0
3 (diradical)	–	–	-	-	–	25.6	–	–	–
4(zwitterion)	−4.0	−6.9	−10.4	−7.1	−7.0	9.7	14.6	17.3	−0.2
TS3 (closing)	−0.2	−3.4	−4.9	−6.3	−6.6	15.1	13.3	18.1	5.5
5	−1.6	−8.7	−15.4	−13.0	−13.0	1.4	4.0	15.6	0.2

[a] Geometry optimized with SMD/B3LYP/6–31+G(d,p). [b] Enthalpy correction at 298 K with SMD/B3LYP/6–31+G(d,p)

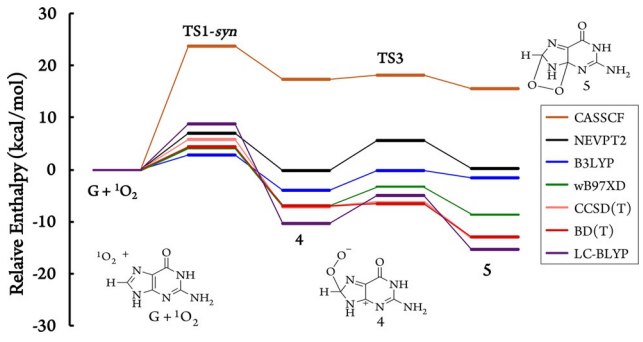

Figure 2. Relative enthalpies for the formation of guanine endoperoxide from *syn*-addition of singlet oxygen to guanine using various levels of theory with the 6–31 + G(d,p) basis set in aqueous solution using SMD. All the spin-contaminated DFT, CCSD(T), and BD(T) energies are spin-projected.

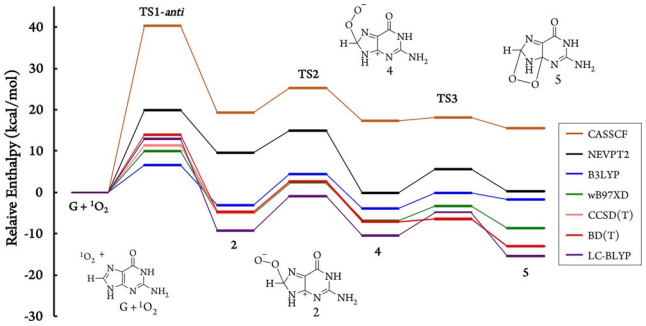

Figure 3. Relative enthalpies for the formation of guanine endoperoxide from *anti*-addition of singlet oxygen to guanine using various levels of theory with the 6–31 + G(d,p) basis set in aqueous solution using SMD. All the spin-contaminated DFT, CCSD(T), and BD(T) energies are spin-projected.

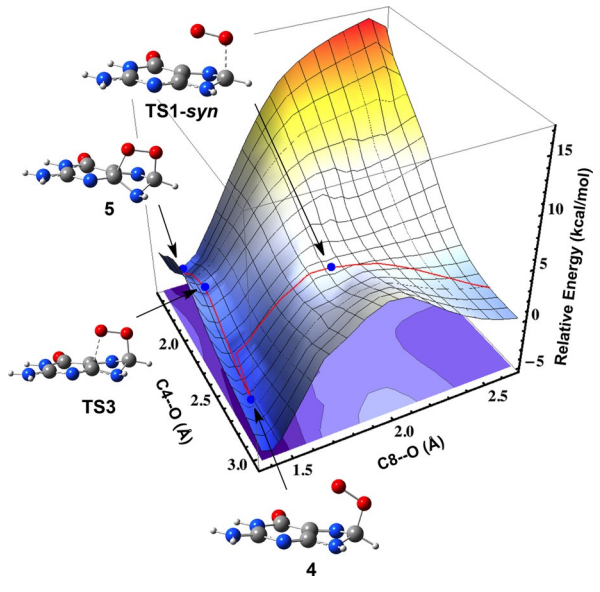

Figure 4. Potential energy surface for singlet oxygen addition to the guanine ring as a function of the C4···O and C8···O distances. The vertical axis shows the energy (without ZPE) in kcal mol^{-1} with respect to the sum of the energies of infinitely separated guanine and singlet oxygen. The surface is calculated with the B3LYP/6–31 + G(d,p) level of theory with SMD solvation and approximate spin projection (see Figure S3 for the surface without spin projection).

ring in guanine. The reaction path descends to the *syn* C8-OO intermediate, which can close to the endoperoxide via a small barrier.

Since the singlet oxygen addition occurs on the imidazole fragment of the guanine, the possibility of the synchronous concerted addition was further explored by comparing with singlet oxygen addition to the methyl-substituted imidazole. We indeed find a synchronous concerted pathway that forms imidazole endoperoxide with a reaction barrier of $\Delta G = 8.9$ kcal mol^{-1} with B3LYP (9.0 kcal mol^{-1} with ωB97XD). This addition barrier is in good agreement with the reported free energy barrier of 8.6 kcal mol^{-1} for histidine using CCSD(T) calculations.[70] This supports the premise that the conjugation in guanine prevents simultaneous addition at C4 and C8, thereby favoring initial addition of the singlet oxygen at C8.

The closed-shell optimized TS for non-synchronous *syn*-addition of singlet oxygen to C8 of guanine has a spin restricted to unrestricted instability. Open-shell optimization shows that **TS1-*syn*** has a small amount of spin contamination ($<S^2> = 0.34$) resulting from mixing with the lower-lying triplet state. After spin projection, the enthalpy barrier is calculated to be 2.8 kcal mol^{-1} with B3LYP (ωB97XD = 4.1 kcal mol^{-1}, CCSD(T) = 5.8 kcal mol^{-1}). Similar to $^1O_2$ + cyclohexadiene, the addition barrier and the energies of the intermediates are too high with CASSCF (Table 2, Figure 2). When dynamic electron correlation is added using NEVPT2, the barrier is in better agreement with the DFT, CCSD(T) and BD(T) calculations.

Intermediate **4** formed by *syn* addition of $^1O_2$ has an elongated O–O bond, 1.48 Å, and a short C8–O bond, 1.37 Å (Figure 1), and is a closed shell structure with no restricted to unrestricted instability and no diradical character. It has a net Mulliken charge of −1.0 on the O–O fragment and +1.0 charge delocalized throughout the guanine ring (mostly on C4-C5-N7), and can thus be characterized as a zwitterion, as found by Dumont et al.[68] Ring closure of **4** to guanine endoperoxide **5** has only a small barrier (B3LYP = 3.8 kcal mol^{-1}, ωB97XD = 3.5 kcal mol^{-1}, CCSD(T) = 0.8 kcal mol^{-1}, NEVPT2 = 5.7 kcal mol^{-1}). Although the B3LYP functional predicts the guanine endoperoxide **5** to be 2.4 kcal mol^{-1} less stable than **4**, the other DFT functionals, CCSD(T), and BD(T) calculations predict the endoperoxide to be more stable than **4** by about 2–6 kcal mol^{-1}. Dumont et al. found similar results for the relative stabilities with wavefunction methods and a variety of density functionals.[67–69]

Closed-shell DFT calculations of the transition state for the *anti*-addition of singlet oxygen at C8 of guanine also have spin restricted to unrestricted instabilities. Optimization of singlet **TS1-*anti*** with open-shell DFT shows strong mixing with the higher spin states ($<S^2> = 1.00$). After spin projection, the enthalpy barriers for the *anti*-addition of singlet oxygen (B3LYP = 6.5 kcal mol^{-1}, ωB97XD = 9.9 kcal mol^{-1}, LC-BLYP = 13.0 kcal mol^{-1}, CCSD(T) = 11.4 kcal mol^{-1}, BD(T) = 14.0 kcal mol^{-1}, NEVPT2 = 19.9 kcal mol^{-1}) are 4–6 kcal mol^{-1} higher than the barriers for *syn*-addition computed at the same level of theory (Table 2, Figure 3). These values are considerably lower than the barriers previously reported for closed shell DFT calculations.[68]

The *anti*-addition of $^1O_2$ can produce two intermediates, a broken symmetry open-shell structure, **1** (with short O–O bond, 1.33 Å, and elongated C8–O bond, 1.51 Å) and a closed-shell structure, **2** (elongated O–O bond, 1.48 Å and short C8–O bond, 1.39 Å). Intermediate **1** is a singlet diradical with one electron in a π^* antibonding orbital of the O–O fragment and the other electron delocalized on the C4-C5-N7 part of the guanine ring. Structure **1** also shows a large amount spin contamination ($<S^2>=1.0$) from the triplet state, and after projection is still approximately 5–10 kcal mol^{-1} higher in energy than **2**. Similar to the *syn*-C8-*O*-O adduct **4**, the closed-shell *anti*-adduct **2** is a zwitterion with a net Mulliken charge of −1.0 on the O–O fragment and +1.0 charge delocalized in the guanine ring (mostly on the C4-C5-N7 fragment). Dumont et al.[68] also found the *anti*-zwitterion to be more stable than the diradical. Rotation around the C8–O bond of the *anti*-adducts **1** and **2** results the formation of the *syn*-adduct, **4**. With open shell DFT, as the O–O fragment in diradical **1** is rotated about C8–O bond to an N9-C8-*O*-O dihedral angle of −176.0°, the singly occupied π^* orbital interacts with the singly occupied π orbital of guanine ring to form the zwitterion intermediate, **4**. The B3LYP barriers for rotation from *anti*- to *syn*- are 2.1 and 7.6 kcal mol^{-1} for **1** and **2**, respectively. Similar rotational barrier was also reported by Dumont et al.[68] For the closed-shell structures such as **2**, **4**, and **5** relative energies calculated with CCSD(T) and BD(T) are expected to be quite reasonable. As shown in Table 2, the relative energies for these closed shell structures calculated with ωB97XD are in good agreement with CCSD(T) and BD(T) whereas the LC-BLYP tends to over-stabilize these structures. The energies of the intermediates are too high with CASSCF, while the NEVPT2 calculations are in somewhat better agreement with the DFT, CCSD(T) and BD(T) (Table 2, Figures 3).

In summary, the stepwise *syn*-addition of the singlet oxygen to guanine to form the endoperoxide is the most favorable pathway, and is preferred over the stepwise *anti*-addition of singlet oxygen by 4–6 kcal mol^{-1}. The barrier for the *syn*-addition of singlet oxygen to the C8 of guanine to form C8-*O*-O-guanine zwitterion intermediate is in the range of 3–8 kcal mol^{-1} and should be the rate-determining step for the formation of the endoperoxide. The barriers for rotation and for ring closure are small and the endoperoxide is more stable than the zwitterionic intermediates. Guanine is the preferred site for $^1O_2$ addition. Corresponding calculations on adenine show that the barriers for $^1O_2$ addition are 3–4 kcal mol^{-1} higher than for guanine, and the formation of the zwitterionic intermediate is endothermic rather than exothermic (see Table S1 and Figures S4, 5 in the Supporting Information).

(c) Reaction of guanine endoperoxide to form 8-oxoG and 8-oxoG^{ox}

Figure 5 shows the relative enthalpies calculated for the pathways shown in Scheme 4. Protonation of 4,8-guanine endoperoxide, **5,** results in the opening of the 5-membered endoperoxide ring to form the 8-OOH-cationic intermediate, **6**. Direct deprotonation from C8 of guanine endoperoxide **5** causes cleavage of O–O bond, resulting the formation of 4O-8-oxoguanine anionic intermediate **6′AN** (Figure 5), which can then be protonated ($pK_a=9.0$) forming **6′**. This process has a forward reaction barrier of 27.3 kcal mol^{-1} for the simultaneous ring opening and the transfer of a proton to the imidazole and is exothermic by 86 kcal mol^{-1}. Alternatively, intermediate **6** can undergo deprotonation from C8 ($pK_a=-13.1$) or from N1 ($pK_a=5.9$) to form neutral intermediates **7** or **7′**, respectively. Loss of the proton from C8 of **6** forming **7** restores the planarity of the guanine framework, hence is calculated to be quite acidic. The transfer of H from N1 of **7** to the OH of C8-OOH and loss of H_2O produces **8-oxoG^{ox}**, **8** (see Scheme 4). Alternatively, as discussed in the literature,[15,25,26] in the presence of reducing agents such as thiols (e.g. glutathione, cysteine, etc.), dimethyl sulfide or Fe^{2+}, the intermediate 8-OOH-guanine, **7** could be reduced to form **8-oxoG**, **8′**. A series of experiments by Burrows and co-workers has shown that the dehydration of **6** is a major pathway leading to the formation of **Sp** in the case of guanine nucleotide.[30,32,34] In the case of double-stranded DNA, however, **7** can be reduced to form **8-oxoG**.[14–19] Reduction of **7** with dimethyl sulfide is calculated to have a reaction barrier of 7.9 kcal mol^{-1}. This indicates that if the reducing agent is present in the solution, the reduction of **7** can be a competitive pathway to form **8-oxoG** (Figure 5). The formation of **8-oxoG^{ox}** via dehydration is calculated to be the more favored pathway (barrierless) over O–O cleavage (barrier height of 27.3 kcal mol^{-1}) or reduction (barrier height of 7.9 kcal mol^{-1} for Me_2S). Therefore, only the reaction of **8-oxoG^{ox}** is included in the following discussion.

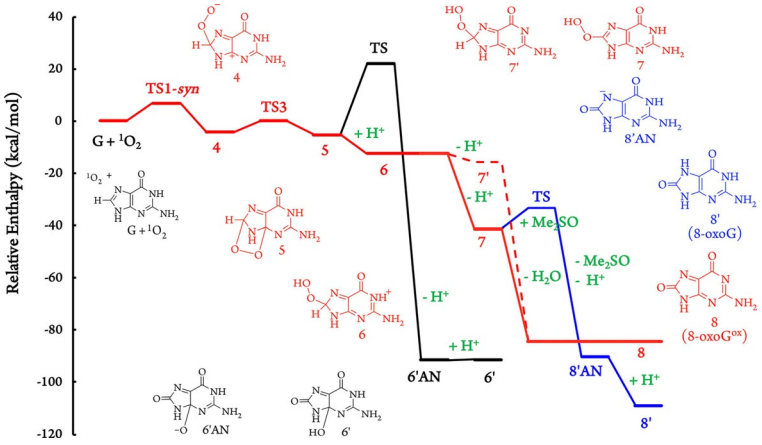

Figure 5. Relative enthalpies for the formation of **8-oxoG** and **8-oxoG^{ox}** from the endoperoxide calculated at the SMD/ωB97XD/aug-cc-pVTZ//SMD/ωB97XD/6–31+G(d,p) level of theory. The solid black line corresponds to the O–O bond cleavage pathway forming **7′**. The solid blue line corresponds to the reduction of intermediate **7** by Me_2S. The red line corresponds to the dehydration pathway leading to form 8-oxoG^{ox}. The solid red line represents the most favored pathway.

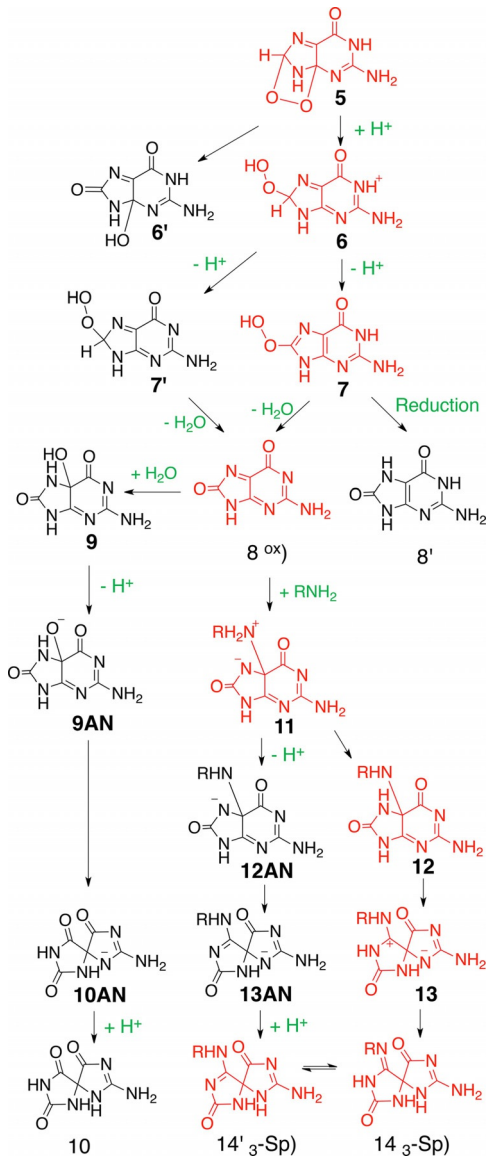

Scheme 4. Pathways for the formation of **8-oxoG**, **8-oxoG^{ox}**, **Sp** and **5-NHCH$_3$-Sp** from guanine endoperoxide via the addition of water or methyl amine (pathway shown in red is the lowest energy).

(d) Nucleophilic addition reaction 8-oxoG^{ox} to form substituted spiroiminodihydantoin

In a second addition step, methylamine or a water molecule can add across the C5–N7 double bond of **8-oxoG^{ox}** (**8**), shown in Scheme 4 and Figure 6, and reported in our previous paper.[54] The addition of water is calculated to have a forward barrier of 7.1 kcal mol^{-1} with ωB97XD (9.6 kcal mol^{-1} with B3LYP) while the addition of methylamine is a barrierless process. The water adduct, **9** loses a proton from C5–OH (pK_a = 6.3) to form an anionic intermediate, **9AN.** Anion **9AN**, then undergoes acyl migration from C5 to C4 of the guanine ring and forms **10AN**, which upon protonation forms the final product, spiroiminodihydantoin, **Sp (10)**.[30,32,78] The C5-methylamine adduct **11**, can directly deprotonate from C5–NH$_2$ and form the anionic intermediate **12AN** (pK_a = 3.0) or undergo tautomerization to form neutral intermediate **12** (barrier height ΔH = 2.9 kcal mol^{-1}. Both **12** and **12AN** can undergo a 1,2 shift of the acyl group. The 1,2 acyl group migration of **12** and a proton rearrangement results the formation of the final tautomeric 5-methylamine-**Sp** products, **14** and **14′ (5-NHCH$_3$-Sp)**. C5-methylamine-Sp, **14** and **14′** are thermodynamically slightly more stable compared to the unsubstituted **Sp**, **10**. Since the barrier calculated for the methylamine addition to C5 of **8-oxoG^{ox}** is significantly lower than the barrier for water addition, 5-NHCH3-Sp (**14′**) should be the dominant reaction product. This result is in good agreement with the experimental finding of **5-Lysine-Sp** (100%)[30] and **5-NH$_2$-Sp** (83%)[34] as the major cross-link products with lysine and ammonia, respectively.

Conclusion

The energetics for the aqueous-phase reaction of guanine with singlet oxygen ($^1\Delta_g$) and the formation of **Sp** and **5-NHCH$_3$-Sp** are shown in Figure 7. The energies have been calculated by DFT (B3LYP and ωB97XD functionals) with SMD implicit solvation. Initial formation of guanine endoperoxide from guanine and singlet oxygen has been further investigated with LC-BLYP, CCSD(T), BD(T), CASSCF and NEVPT2 calculations. Open-shell DFT, CCSD(T) and BD(T) calculations of singlet oxygen have significant spin-contamination from the lower-lying triplet state. The spin-contamination is not limited to the singlet oxygen but is also present in some of the TSs and intermediates. Spin-pure states are obtained by using Yamaguchi's approximate spin-projection method and by CASSCF and NEVPT2 calculations. The addition of singlet oxygen to guanine is favored over addition to adenine by 3–4 kcal mol^{-1}. The formation of guanine endoperoxide proceeds in a step-wise fashion and the zwitterionic pathway is favored over the diradical pathway by more than 5 kcal mol^{-1}. The singlet oxygen can add to C8 of guanine either *syn* and *anti* with respect to the guanine ring. The barrier calculated for the *syn*-addition of singlet oxygen is 4–6 kcal mol^{-1} lower than for *anti*-addition. The initial addition of singlet oxygen is the rate limit step since the barrier for the ring closure of the zwitterion intermediate is smaller than for the initial addition of singlet oxygen. The opening of the endoperoxide ring in **5** through protonation at C4–O to form protonated intermediate **6** is strongly favored over the O–O bond cleavage to form 4-hydroxy-8-oxo-guanine **6′**. Deprotonation of C8 in the 8-OOH-guanine cationic intermediate **6** produces 8-hydroperoxyguanine, **7**. Loss of a water molecule after proton rearrangement forms oxidized 8-oxoguanine (**8-oxoG^{ox}**). In the presence of a suitable reducing agent, the reduction of **7** could compete with dehydration, leading to the formation of the thermodynamically more stable intermediate **8-oxoG** observed in the experiments. The barrier for the methylamine addition across the C5–N7 double bond of **8-oxoG^{ox}** (**8**) is significantly lower than for the water addition. The methylamine-adduct and water-adduct undergo further rearrangement reactions to produce final products **5-NHCH$_3$-Sp** and **Sp**. Based on the energetics calculated here, **5-NHCH$_3$-Sp** should be the dominant product. Our observations are in good agree-

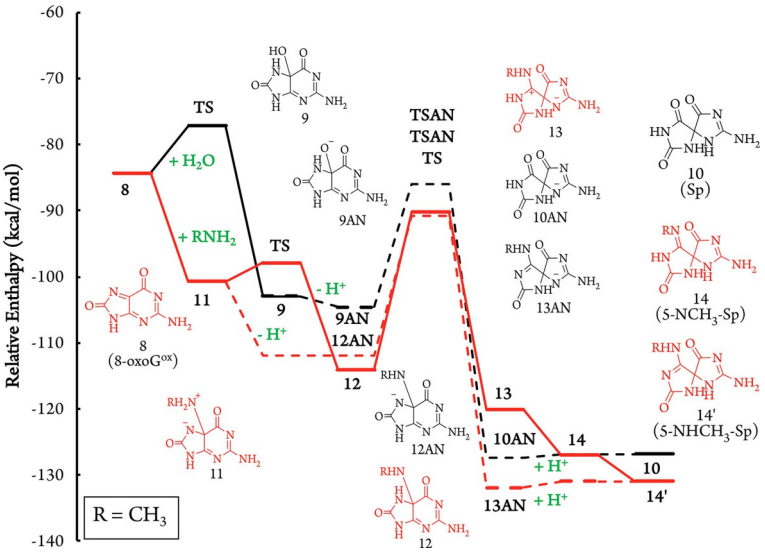

Figure 6. Relative enthalpies for the formation of Sp and 5-$NHCH_3$-Sp from the addition of water or methylamine to 8-oxoG^{ox} calculated at the SMD/ωB97XD/aug-cc-pVTZ//SMD/ωB97XD/6–31 + G(d,p) level of theory. The black line corresponds to the addition of water and the red line corresponds to the addition of a methylamine. Pathways involving anions are shown as dashed lines. The solid red line represents the most favored pathway. The pathways leading to the structure **8** are shown in Figure 5.

ment with the available experimental results.[30,34] Lowering the pH of solution would decrease the concentration of unprotonated methylamine, thereby favoring the formation of **Sp** or **Gh** over **5-$NHCH_3$-Sp**.

Computational Methods

Geometries were optimized with B3LYP,[79–81] LC-BLYP[80–82] and ωB97XD[83] density functional methods in aqueous solution using the 6–31 + G(d,p)[84–88] basis set and the SMD[89] implicit solvation model for aqueous solution. Optimized geometries were confirmed to be minima with no imaginary frequencies. Transition states (TSs) were verified to have only one imaginary frequency with a vibrational mode corresponding to the movement from reactants to products. The transition states were further tested by calculating the intrinsic reaction coordinate (IRC) to connect the transition state with reactants and products.[90,91] Transition states for the addition of nucleophiles across a double bond included an explicit water molecule. When assisted by an additional water molecule, these transition states are six-membered rings and have significantly lower barriers compared to non-assisted transition states with four-membered rings. The deprotonation and protonation processes were modeled by using imidazole and imidazolium (pK_a 6.9) as a proton accepter and donor, respectively, as a computational equivalent to an experimental buffer of pH 7. More accurate single point energies were calculated using the aug-cc-pVTZ basis set[92] in aqueous solution using the geometries optimized with the 6–31 + G(d,p) basis set. Since reactions with singlet oxygen may involve structures with multi-reference character, transition states and intermediates for the formation of guanine endoperoxide were also optimized using complete active space self-consistent field (CASSCF)[93–96] calculations with an active space of 20 electrons and 14 orbitals (see Figure S1 in the Supporting Information for the details of the orbitals). Additional energy calculations for the formation of guanine endoperoxide were obtained using CCSD(T),[97,98]

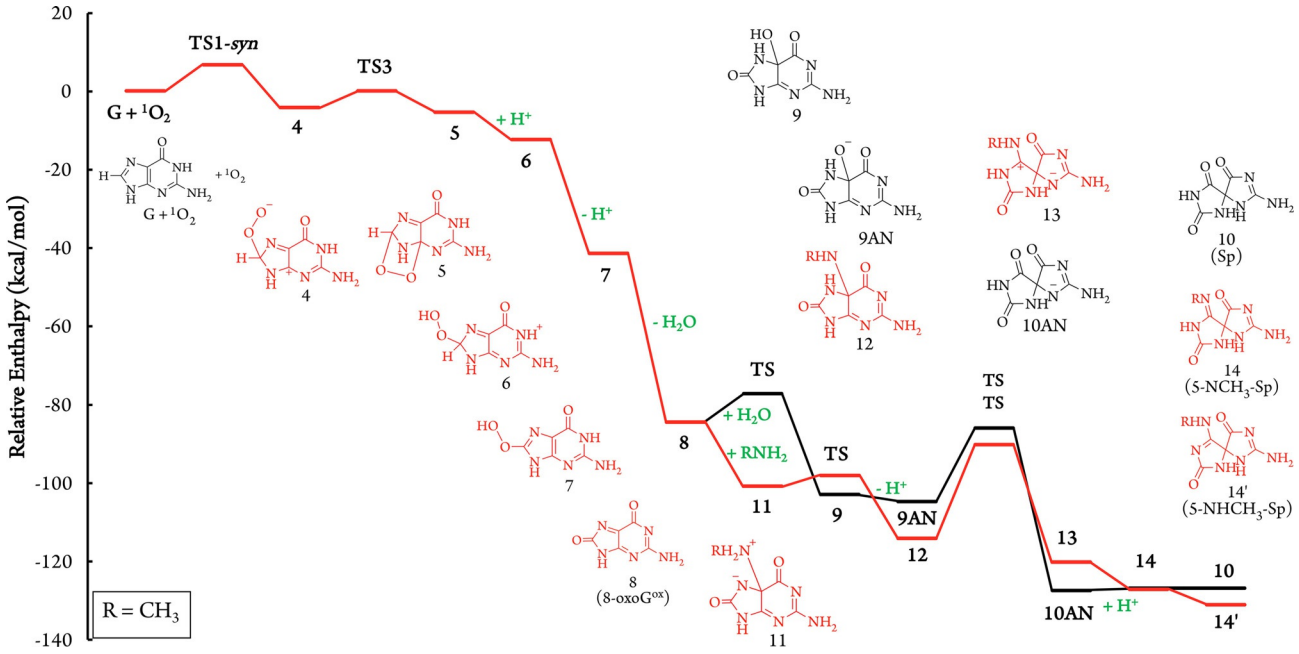

Figure 7. Summary of the lowest energy pathway for the formation of **Sp** and **5-$NHCH_3$-Sp** from the singlet oxygen addition to the guanine ring followed by the nucleophilic addition of water or methylamine. Relative enthalpies (kcal mol^{-1}) are calculated with SMD-ωB97XD/aug-cc-pVTZ//SMD-ωB97XD/6–31 + G(d,p) level of theory. The spin contamination in singlet oxygen, TSs and intermediates are corrected with the Yamaguchi approximate spin projection method. The black line on the left corresponds to the addition of water and the red line corresponds to the methylamine addition. The solid red line represents the most favored pathway.

BD(T),[99] CASSCF (14 electrons in 11 orbitals active space and 20 electrons in 14 orbitals active space, see SI for details), and NEVPT2[100,101] (14 electrons and 11 orbitals active space) single point computations with the 6–31+G(d,p) basis set and the SMD/B3LYP/6–31+G(d,p) optimized geometries. Most calculations were carried out with the development version of Gaussian series of programs;[102] the NEVPT2 calculations were carried out with ORCA.[103]

Spin-unrestricted DFT, CCSD(T), and BD(T) calculations of open shell singlets may have significant spin contamination from the lowest triplet states. The energies of spin contaminated broken symmetry (BS) calculations have been corrected using Yamaguchi's approximate spin projection (AP) method.[63,65] The spin-projected total energy of a singlet state (E^{AP}) is given by Equation 1:

$$E^{AP} = \alpha E^{BS} - \beta E^{HS} \quad (1)$$

in which

$$\alpha = \frac{\langle S^2 \rangle^{HS}}{\langle S^2 \rangle^{HS} - \langle S^2 \rangle^{BS}}$$

$$\beta = \frac{\langle S^2 \rangle^{BS}}{\langle S^2 \rangle^{HS} - \langle S^2 \rangle^{BS}}$$

E^{BS} is the energy of broken symmetry, spin unrestricted singlet state and E^{HS} is the energy of the high spin (triplet) state. The spin contamination in the triplet state is assumed to be negligible.

Acknowledgements

This work was supported by grants from the National Science Foundation (CHE1464450 to H.B.S. and CHE1507813 to C.J.B.). BT thanks Wayne State University for a Thomas C. Rumble Fellowship and a Frank Knoller Fellowship. We also thank Wayne State University C&IT for use of the computing grid.

Conflict of interest

The authors declare no conflict of interest.

Keywords: DNA · DNA–protein cross-link · endoperoxide · guanine · singlet oxygen

[1] A. Held, D. Halko, J. Hurst, *J. Am. Chem. Soc.* **1978**, *100*, 5732–5740.
[2] P. Di Mascio, E. J. Bechara, M. H. Medeiros, K. Briviba, H. Sies, *FEBS Lett.* **1994**, *355*, 287–289.
[3] C. Pierlot, J.-M. Aubry, K. Briviba, H. Sies, P. Di Mascio, *Methods Enzymol.* **2000**, *319*, 3–20.
[4] J. R. Kanofsky, *Chem.-Biol. Interact.* **1989**, *70*, 1–28.
[5] M. C. DeRosa, R. J. Crutchley, *Coord. Chem. Rev.* **2002**, *233–234*, 351–371.
[6] A. P. Breen, J. A. Murphy, *Free Radical Biol. Med.* **1995**, *18*, 1033–1077.
[7] C. J. Burrows, J. G. Muller, *Chem. Rev.* **1998**, *98*, 1109–1152.
[8] D. Wang, D. A. Kreutzer, J. M. Essigmann, *Mutat. Res.* **1998**, *400*, 99–115.
[9] K. B. Beckman, B. N. Ames, *Mutat. Res. Mut.* **1999**, *424*, 51–58.
[10] P. Hasty, J. Campisi, J. Hoeijmakers, H. van Steeg, J. Vijg, *Science* **2003**, *299*, 1355–1359.
[11] T. Gimisis, C. Cismaş, *Eur. J. Org. Chem.* **2006**, 1351–1378.
[12] S. Perrier, J. Hau, D. Gasparutto, J. Cadet, A. Favier, J.-L. Ravanat, *J. Am. Chem. Soc.* **2006**, *128*, 5703–5710.
[13] A. M. Fleming, C. J. Burrows, *Free Radical Biol. Med.* **2017**, DOI: 10.1016/j.freeradbiomed.2016.1011.1030.
[14] G. R. Martinez, A. P. M. Loureiro, S. A. Marques, S. Miyamoto, L. F. Yamaguchi, J. Onuki, E. A. Almeida, C. C. M. Garcia, L. F. Barbosa, M. H. G. Medeiros, P. Di Mascio, *Mutat. Res.* **2003**, *544*, 115–127.
[15] J.-L. Ravanat, G. R. Martinez, M. H. G. Medeiros, P. Di Mascio, J. Cadet, *Arch. Biochem. Biophys.* **2004**, *423*, 23–30.
[16] W. L. Neeley, J. M. Essigmann, *Chem. Res. Toxicol.* **2006**, *19*, 491–505.
[17] G. Pratviel, B. Meunier, *Chem. Eur. J.* **2006**, *12*, 6018–6030.
[18] J. Cadet, T. Douki, J.-L. Ravanat, *Free Radical Biol. Med.* **2010**, *49*, 9–21.
[19] J. Cadet, T. Douki, J.-L. Ravanat, P. Di Mascio, *Singlet Oxygen: Applications in Biosciences and Nanosciences Volume* **2016**, *1*, 393.
[20] J. Cadet, K. J. A. Davies, M. H. G. Medeiros, P. Di Mascio, J. R. Wagner, *Free Radical Biol. Med.* **2017**, DOI: 10.1016/j.freeradbiomed.2016.1012.1049.
[21] A. M. Fleming, C. J. Burrows, *Chem. Res. Toxicol.* **2013**, *26*, 593–607.
[22] C. Sheu, C. S. Foote, *J. Am. Chem. Soc.* **1993**, *115*, 10446–10447.
[23] T. P. Devasagayam, S. Steenken, M. S. Obendorf, W. A. Schulz, H. Sies, *Biochemistry* **1991**, *30*, 6283–6289.
[24] G. R. Martinez, J. L. Ravanat, J. Cadet, M. H. G. de Medeiros, P. Di Mascio, *J. Mass Spectrom.* **2007**, *42*, 1326–1332.
[25] J. E. McCallum, C. Y. Kuniyoshi, C. S. Foote, *J. Am. Chem. Soc.* **2004**, *126*, 16777–16782.
[26] P. S. Peres, A. Valerio, S. M. Cadena, S. M. Winnischofer, A. C. Scalfo, P. Di Mascio, G. R. Martinez, *Arch. Biochem. Biophys.* **2015**, *586*, 33–44.
[27] J.-L. Ravanat, J. Cadet, *Chem. Res. Toxicol.* **1995**, *8*, 379–388.
[28] J.-L. Ravanat, S. Sauvaigo, S. Caillat, G. R. Martinez, M. H. Medeiros, P. D. Mascio, A. Favier, J. Cadet, *Biol. Chem.* **2004**, *385*, 17–20.
[29] J. L. Ravanat, C. Saint-Pierre, P. Di Mascio, G. R. Martinez, M. H. Medeiros, J. Cadet, *Helv. Chim. Acta* **2001**, *84*, 3702–3709.
[30] X. Xu, J. G. Muller, Y. Ye, C. J. Burrows, *J. Am. Chem. Soc.* **2008**, *130*, 703–709.
[31] J. C. Niles, J. S. Wishnok, S. R. Tannenbaum, *Org. Lett.* **2001**, *3*, 963–966.
[32] Y. Ye, J. G. Muller, W. Luo, C. L. Mayne, A. J. Shallop, R. A. Jones, C. J. Burrows, *J. Am. Chem. Soc.* **2003**, *125*, 13926–13927.
[33] J. Cadet, T. Douki, D. Gasparutto, J.-L. Ravanat, *Mutat. Res.* **2003**, *531*, 5–23.
[34] A. M. Fleming, E. I. Armentrout, J. Zhu, J. G. Muller, C. J. Burrows, *J. Org. Chem.* **2015**, *80*, 711–721.
[35] Y. Sun, W. Lu, J. Liu, *J. Phys. Chem. B* **2017**, *121*, 956–966.
[36] B. Morin, J. Cadet, *J. Am. Chem. Soc.* **1995**, *117*, 12408–12415.
[37] B. Morin, J. Cadet, *Chem. Res. Toxicol.* **1995**, *8*, 792–799.
[38] A. Zhitkovich, V. Voitkun, M. Costa, *Biochemistry* **1996**, *35*, 7275–7282.
[39] K. L. Nguyen, M. Steryo, K. Kurbanyan, K. M. Nowitzki, S. M. Butterfield, S. R. Ward, E. D. A. Stemp, *J. Am. Chem. Soc.* **2000**, *122*, 3585–3594.
[40] S. K. Chakrabarti, C. Bai, K. S. Subramanian, *Toxicol. Appl. Pharmacol.* **2001**, *170*, 153–165.
[41] K. Kurbanyan, K. L. Nguyen, P. To, E. V. Rivas, A. M. K. Lueras, C. Kosinski, M. Steryo, A. González, D. A. Mah, E. D. A. Stemp, *Biochemistry* **2003**, *42*, 10269–10281.
[42] M. E. Johansen, J. G. Muller, X. Xu, C. J. Burrows, *Biochemistry* **2005**, *44*, 5660–5671.
[43] G. Sun, C. J. Fecko, R. B. Nicewonger, W. W. Webb, T. P. Begley, *Org. Lett.* **2006**, *8*, 681–683.
[44] M. J. Solivio, T. J. Joy, L. Sallans, E. J. Merino, *J. Inorg. Biochem.* **2010**, *104*, 1000–1005.
[45] S. Wickramaratne, S. Mukherjee, P. W. Villalta, O. D. Schärer, N. Y. Tretyakova, *Bioconjugate Chem.* **2013**, *24*, 1496–1506.
[46] K. V. Petrova, A. D. Millsap, D. F. Stec, C. J. Rizzo, *Chem. Res. Toxicol.* **2014**, *27*, 1019–1029.
[47] S. Silerme, L. Bobyk, M. Taverna-Porro, C. Cuier, C. Saint-Pierre, J.-L. Ravanat, *Chem. Res. Toxicol.* **2014**, *27*, 1011–1018.
[48] Y. Uvaydov, N. E. Geacintov, V. Shafirovich, *Phys. Chem. Chem. Phys.* **2014**, *16*, 11729–11736.
[49] G. F. Strniste, S. C. Rall, *Biochemistry* **1976**, *15*, 1712–1719.
[50] E. R. Blazek, P. V. Hariharan, *Photochem. Photobiol.* **1984**, *40*, 5–13.

[51] N. Ramakrishnan, M. E. Clay, L. Y. Xue, H. H. Evans, A. Rodriguezantunez, *Photochem. Photobiol.* **1988**, *48*, 297 – 303.
[52] S. A. Altman, T. H. Zastawny, L. Randers-Eichhorn, M. A. Cacciuttolo, S. A. Akman, M. Dizdaroglu, G. Rao, *Free Radical Biol. Med.* **1995**, *19*, 897 – 902.
[53] S. Barker, M. Weinfeld, D. Murray, *Mutat. Res.* **2005**, *589*, 111 – 135.
[54] B. Thapa, B. H. Munk, C. J. Burrows, H. B. Schlegel, *Chem. Res. Toxicol.* **2016**, *29*, 1396 – 1409.
[55] F. Bernardi, A. Bottoni, M. Olivucci, M. A. Robb, H. B. Schlegel, G. Tonachini, *J. Am. Chem. Soc.* **1988**, *110*, 5993 – 5995.
[56] B. S. Jursic, Z. Zdravkovski, *J. Org. Chem.* **1995**, *60*, 2865 – 2869.
[57] M. Bobrowski, A. Liwo, S. Oldziej, D. Jeziorek, T. Ossowski, *J. Am. Chem. Soc.* **2000**, *122*, 8112 – 8119.
[58] F. Sevin, M. L. McKee, *J. Am. Chem. Soc.* **2001**, *123*, 4591 – 4600.
[59] A. G. Leach, K. N. Houk, *Chem. Commun.* **2002**, 1243 – 1255.
[60] D. A. Singleton, C. Hang, M. J. Szymanski, M. P. Meyer, A. G. Leach, K. T. Kuwata, J. S. Chen, A. Greer, C. S. Foote, K. N. Houk, *J. Am. Chem. Soc.* **2003**, *125*, 1319 – 1328.
[61] S.-H. Chien, M.-F. Cheng, K.-C. Lau, W.-K. Li, *J. Phys. Chem. A* **2005**, *109*, 7509 – 7518.
[62] A. R. Reddy, M. Bendikov, *Chem. Commun.* **2006**, 1179 – 1181.
[63] T. Saito, S. Nishihara, Y. Kataoka, Y. Nakanishi, T. Matsui, Y. Kitagawa, T. Kawakami, M. Okumura, K. Yamaguchi, *Chem. Phys. Lett.* **2009**, *483*, 168 – 171.
[64] J. L. Sonnenberg, H. P. Hratchian, H. B. Schlegel, in *Computational Inorganic and Bioinorganic Chemistry* (Ed.: E. I. S. Solomon, R. A.; King, R. B.), Wiley, Chichester, **2009**, pp. 173 – 186.
[65] T. Saito, S. Nishihara, Y. Kataoka, Y. Nakanishi, Y. Kitagawa, T. Kawakami, S. Yamanaka, M. Okumura, K. Yamaguchi, *J. Phys. Chem. A* **2010**, *114*, 7967 – 7974.
[66] X. Song, M. G. Fanelli, J. M. Cook, F. Bai, C. A. Parish, *J. Phys. Chem. A* **2012**, *116*, 4934 – 4946.
[67] R. Grüber, A. Monari, E. Dumont, *J. Phys. Chem. A* **2014**, *118*, 11612 – 11619.
[68] E. Dumont, R. Grüber, E. Bignon, C. Morell, Y. Moreau, A. Monari, J.-L. Ravanat, *Nucleic Acids Res.* **2016**, *44*, 56 – 62.
[69] E. Dumont, R. Grüber, E. Bignon, C. Morell, J. Aranda, J. L. Ravanat, I. Tuñón, *Chem. Eur. J.* **2016**, *22*, 12358 – 12362.
[70] J. Méndez-Hurtado, R. López, D. Suárez, M. I. Menéndez, *Chem. Eur. J.* **2012**, *18*, 8437 – 8447.
[71] W. Lu, H. Teng, J. Liu, *Phys. Chem. Chem. Phys.* **2016**, *18*, 15223 – 15234.
[72] W. Lu, J. Liu, *Chem. Eur. J.* **2016**, *22*, 3127 – 3138.
[73] E. Lissi, M. Encinas, E. Lemp, M. Rubio, *Chem. Rev.* **1993**, *93*, 699 – 723.
[74] K. Yamaguchi, Y. Takahara, T. Fueno, K. Houk, *Theor. Chim. Acta* **1988**, *73*, 337 – 364.
[75] K. Yamaguchi, M. Okumura, W. Mori, J. Maki, K. Takada, T. Noro, K. Tanaka, *Chem. Phys. Lett.* **1993**, *210*, 201 – 210.
[76] S. Yamanaka, M. Okumura, M. Nakano, K. Yamaguchi, *J. Mol. Struct.* **1994**, *310*, 205 – 218.
[77] R. Ashford, E. Ogryzlo, *Can. J. Chem.* **1974**, *52*, 3544 – 3548.
[78] B. H. Munk, C. J. Burrows, H. B. Schlegel, *J. Am. Chem. Soc.* **2008**, *130*, 5245 – 5256.
[79] A. D. Becke, *J. Chem. Phys.* **1993**, *98*, 5648 – 5652.
[80] A. D. Becke, *Phys. Rev. A* **1988**, *38*, 3098 – 3100.
[81] C. Lee, W. Yang, R. G. Parr, *Phys. Rev. B* **1988**, *37*, 785 – 789.
[82] H. Iikura, T. Tsuneda, T. Yanai, K. Hirao, *J. Chem. Phys.* **2001**, *115*, 3540 – 3544.
[83] J.-D. Chai, M. Head-Gordon, *Phys. Chem. Chem. Phys.* **2008**, *10*, 6615 – 6620.
[84] R. Ditchfield, W. J. Hehre, J. A. Pople, *J. Chem. Phys.* **1971**, *54*, 724 – 728.
[85] W. J. Hehre, R. Ditchfield, J. A. Pople, *J. Chem. Phys.* **1972**, *56*, 2257 – 2261.
[86] P. C. Hariharan, J. A. Pople, *Theor. Chim. Acta* **1973**, *28*, 213 – 222.
[87] M. M. Francl, W. J. Pietro, W. J. Hehre, J. S. Binkley, M. S. Gordon, D. J. DeFrees, J. A. Pople, *J. Chem. Phys.* **1982**, *77*, 3654 – 3665.
[88] T. Clark, J. Chandrasekhar, G. W. Spitznagel, P. V. R. Schleyer, *J. Comput. Chem.* **1983**, *4*, 294 – 301.
[89] A. V. Marenich, J. C. Cramer, D. G. Truhlar, *J. Phys. Chem. B* **2009**, *113*, 6378 – 6396.
[90] K. Fukui, *Acc. Chem. Res.* **1981**, *14*, 363 – 368.
[91] H. P. Hratchian, H. B. Schlegel, in *Theory and applications of computational chemistry* (Eds.: E. G. Scuseria, C. E. Dykstra, G. Frenking, K. S. Kim), Elsevier, Amsterdam, **2005**, pp. 195 – 249.
[92] R. A. Kendall, T. H. Dunning Jr., R. J. Harrison, *J. Chem. Phys.* **1992**, *96*, 6796 – 6806.
[93] P. Siegbahn, A. Heiberg, B. Roos, B. Levy, *Phys. Scr.* **1980**, *21*, 323.
[94] B. O. Roos, P. R. Taylor, P. E. Siegbahn, *Chem. Phys.* **1980**, *48*, 157 – 173.
[95] B. O. Roos, *Int. J. Quantum Chem.* **2009**, *18*, 175 – 189.
[96] J. Olsen, B. O. Roos, P. Jo, H. Jo, *J. Chem. Phys.* **1988**, *89*, 2185 – 2192.
[97] R. J. Bartlett, *Annu. Rev. Phys. Chem.* **1981**, *32*, 359 – 401.
[98] K. Raghavachari, G. W. Trucks, J. A. Pople, M. Head-Gordon, *Chem. Phys. Lett.* **1989**, *157*, 479 – 483.
[99] N. C. Handy, J. A. Pople, M. Head-Gordon, K. Raghavachari, G. W. Trucks, *Chem. Phys. Lett.* **1989**, *164*, 185 – 192.
[100] C. Angeli, R. Cimiraglia, S. Evangelisti, T. Leininger, J.-P. Malrieu, *J. Chem. Phys.* **2001**, *114*, 10252 – 10264.
[101] C. Angeli, R. Cimiraglia, J.-P. Malrieu, *J. Chem. Phys.* **2002**, *117*, 9138 – 9153.
[102] M. J. Frisch, G. W. Trucks, H. B. Schlegel, G. E. Scuseria, M. A. Robb, J. R. Cheeseman, G. Scalmani, V. Barone, B. Mennucci, G. A. Petersson, H. Nakatsuji, M. Caricato, X. Li, H. P. Hratchian, A. F. Izmaylov, J. Bloino, B. G. Janesko, F. Lipparini, G. Zheng, J. L. Sonnenberg, W. Liang, M. Hada, M. Ehara, R. F. K. Toyota, J. Hasegawa, M. Ishida, T. Nakajima, Y. Honda, O. Kitao, H. Nakai, T. Vreven, J. J. A. Montgomery, J. E. Peralta, F. Ogliaro, M. Bearpark, J. J. Heyd, E. Brothers, K. N. Kudin, V. N. Staroverov, T. Keith, R. Kobayashi, J. Normand, K. Raghavachari, A. Rendell, J. C. Burant, S. S. Iyengar, J. Tomasi, M. Cossi, N. Rega, J. M. Millam, M. Klene, J. E. Knox, J. B. Cross, V. Bakken, C. Adamo, J. Jaramillo, R. Gomperts, R. E. Stratmann, O. Yazyev, A. J. Austin, R. Cammi, C. Pomelli, J. W. Ochterski, R. L. Martin, K. Morokuma, V. G. Zakrzewski, G. A. Voth, P. Salvador, J. J. Dannenberg, S. Dapprich, P. V. Parandekar, N. J. Mayhall, A. D. Daniels, O. Farkas, J. B. Foresman, J. V. Ortiz, J. Cioslowski, D. J. Fox, Gaussian Development Version, H.35, Gaussian, Inc., Wallingford, CT, **2014**.
[103] The ORCA program system, F. Neese, *WIREs Comput. Mol. Sci.* **2012**, *2*, 73 – 78.

Manuscript received: January 16, 2017
Accepted Article published: March 1, 2017
Final Article published: April 5, 2017